Evaluation of a Compound Probability Model With Tower-Mounted Scatterometer Data

Benjamin E. Barrowes and David G. Long, *Senior Member, IEEE*

***Abstract*—Six months of data from the YSCAT94 experiment conducted at the CCIW WAVES research platform on Lake Ontario, Canada, are analyzed to evaluate a compound probability model. YSCAT was an ultrawideband small footprint (≈1 m) microwave scatterometer that operated at frequencies of 2–18 GHz, incidence angles from 0° to 60°, both h-pol and v-pol, and which tracked the wind using simultaneous weather measurements. The probability distribution function of the measured instantaneous backscattered amplitude ($p(a)$) is compared to theoretical distributions developed from the composite model and a simple wave spectrum. Model parameters of the resulting Rayleigh/generalized lognormal distribution probability density function (pdf) (C, a_1, and a_2) are derived directly from the data and are found to demonstrate relationships with wind speed, incidence angle, and radar frequency.**

***Index Terms*—Generalized lognormal distribution, microwave scatterometer, sea surface scattering, small-footprint scatterometer.**

I. Introduction

THE PRINCIPAL application for scatterometers is ocean microwave anemometry, i.e., wind speed estimation over bodies of water through radar cross section measurements. The relationship between the environmental parameters of the air–sea interface and the observed radar cross section (σ°) is referred to as the geophysical model function (GMF). Understanding the GMF is central in interpreting scatterometer data. However, it remains poorly understood due to the complexity of the air–sea interface. The normalized radar cross section σ° of the sea surface is dependent on many parameters including incidence angle, microwave frequency, transmit and receive polarizations, wind direction, long wave field, salinity of the water, water temperature, air temperature, and other factors [1]. Tower-mounted scatterometers such as YSCAT are deployed in an effort to better describe the geophysical model function and aid in the understanding of the relationship between environmental parameters and radar backscatter. This paper focuses on the probability distribution of the instantaneous amplitude of electromagnetic backscatter ($p(a)$) from a wind-roughened water surface.

Manuscript received January 30, 2001; revised September 20, 2001. This work was supported in part by grants from the Rocky Mountain NASA Space Grant Consortium.

B. E. Barrowes is with the Center for Electromagnetic Theory and Applications, Massachusetts Institute of Technology, Cambridge, MA 02139-4307 USA (e-mail: barrowes@mit.edu).

D. G. Long is with the Microwave Earth Remote Sensing Laboratory, Brigham Young University, Provo, UT 84602 USA (e-mail: long@byu.edu).

Publisher Item Identifier S 0196-2892(02)01405-5.

A brief summary of the YSCAT instrument and the YSCAT94 experiment is provided in Section II. In Section III, $p(a)$ is modeled by a conditional probability [see (2)] following the development in [2]. The distribution for $p(a|\sigma^\circ)$ is discussed in Section III-A-1, while $p(\sigma^\circ)$ is derived for both the h-pol and v-pol cases in Section III-A-2. In Section IV the resulting distribution for $p(a)$, referred to as a Rayleigh/generalized lognormal distribution (R/gln), is calculated numerically using these distributions for $p(a|\sigma^\circ)$ and $p(\sigma^\circ)$ and then compared to YSCAT94 data sorted according to frequency, polarization, wind direction (upwind or downwind), incidence angle, and wind speed. This is followed by a summary and conclusion.

II. YSCAT Instrument

YSCAT is a tower mounted microwave scatterometer designed to collect normalized radar cross section (σ°) measurements of the sea surface under varying radar and environmental parameters [3]. For this study, YSCAT gathered data at frequencies of 2 GHz (S-band), 3 GHz (S-band), 5 GHz (C-band), 10 GHz (X-band), and 14 GHz (K_u-band) and at incidence angles of 0° (nadir), 10°, 20°, 25°, 30°, 40°, 50°, and 60° is analyzed. YSCAT's antenna was specially designed to provide a fixed beamwidth of approximately five degrees over most of its 2–18 GHz operating bandwidth. Mounted 10 m above the water surface of Lake Ontario, Canada, during the YSCAT94 experiment, the antenna footprint diameter was approximately 1 m for midrange incidence angles. YSCAT could transmit and receive at both horizontal and vertical polarizations and tracked the wind direction with the aid of simultaneous weather data acquired at the site. In this paper, "upwind" and "downwind" include ±20° of the wind direction. *In situ* measurements of wind speed, wind direction, rainfall, and water temperature measurements were also recorded. For a more detailed description of YSCAT, the reader is referred to [3] and [4]. A summary of YSCAT's RF parameters is provided in Table I.

The YSCAT94 experiment consists of data collected by the YSCAT instrument when it was deployed for a period of six months, from June to November, 1994 on the WAVES research platform operated by the Canada Centre for Inland Waters (CCIW) about 1.1 km from the western shore of Lake Ontario. Water depth at this site is about 12 m, and the annual variation in water depth is less that 0.5 m. There are no significant tides, seiches, or associated currents, and other random currents are typically less than 10 cm/s. The CCIW tower was designed to minimize both wind and wave disruption [1] and therefore no effort is made to account for turbulence on the wind and the waves caused by the tower. Prevailing winds in this area were

TABLE I
YSCAT RF SYSTEM PARAMETERS

Center Frequency	2-18 GHz
Peak Output Power	23 dBm
Transmit Polarization	V or H
Two-Way Antenna Beam width	5-10°
Receive Polarization	V or H
Polarization Isolation	15-20 dB
Dynamic Range	60 dB
Baseband Signal Bandwidth	900 Hz

TABLE II
COUNT OF VALID YSCAT94 σ° MEASUREMENTS

Polarization	Frequency	Wind Speed (m/s)			
	(GHz)	0-5	5-7.5	7.5-10	> 10
H	2	4245	1196	516	587
H	3	3808	810	388	299
H	5	7263	1756	791	806
H	10	3739	833	369	308
H	14	6775	1763	744	828
V	2	4315	1502	511	396
V	3	4658	1539	555	366
V	5	10083	3319	1179	622
V	10	6176	2001	636	310
V	14	8595	3064	1034	499

westerly, which provided fetches from 1.1–2 km. Due to this short fetch, waves with periods of four seconds were common, while waves with periods of 8 s or more were rare [4].

The data from the YSCAT94 experiment analyzed in this paper consist of one minute backscatter amplitude (a) records measured at a 2 kHz sampling rate. The 2 kHz power measurements are averaged to yield a data rate of 10 Hz. This integration time of 100 ms is long compared to the coherence time of the waves on the scale of interest and therefore may effect our estimated backscatter distributions, especially at low amplitudes where spikes may dominate the otherwise small average. Radar cross sections (σ°) were calculated from these records, and were binned according to frequency, polarization, wind direction (upwind or downwind), incidence angle, and wind speed. The vast majority of one minute backscatter amplitude records were measured during steady wind conditions leading to stable σ° values. However, one minute data records with means far removed from the aggregate mean of that data bin were generally found to have fluctuating wind speed measurements and unstable σ° values and were therefore discarded. Data collected during or after rainy periods and data corrupted by equipment failures or other sources of error (e.g., ships, birds) were also removed. Table II summarizes the resulting number of σ° measurements in each data bin after these data records were discarded. To reduce errors introduced by receiver gain fluctuation due to temperature changes, distance variations from the water surface, or other factors, each one minute data record was first normalized by dividing by the mean of that individual record. Subsequently, all one minute data records in that bin were multiplied by the aggregate mean of all one minute data records in that bin.

III. YSCAT94 BACKSCATTER DISTRIBUTIONS

The most common model for sea scattered radar return at moderate incidence angles is the composite model. The composite model assumes that the sea surface is composed of small independent patches each of which has a normalized radar cross section (σ°) given by small perturbation theory (SPT) as [1], [5]

$$\sigma^\circ = 16\pi k_m^4 |g_{pp}(\theta_i)|^2 \Psi(2k_m \sin\theta_i,\, 0) \tag{1}$$

where σ° is the normalized radar cross section, θ_i is the incidence angle, $g_{pp}(\theta_i)$ is a polarization dependent reflection coefficient with pp being either hh or vv, k_m is the microwave wavenumber, and Ψ is the wave height spectral density evaluated at the Bragg wavelength $k_b = 2k_m \sin(\theta_i)$.

These patches of relatively small waves (on the order of centimeters), are modulated, or tilted, by larger waves with wavelengths typically on the order of meters. Consequently, the radar cross section distribution depends on the distribution of the long wave field. Following Gotwols and Thompson [2], the compound probability model is reviewed and extended in the remainder of this section.

A. Compound Probability Model

The compound probability model, originally proposed by Valenzuela and Laing [6], considers the aforementioned two scales of waves separately. According to the model, the radar cross section σ° of the sea surface depends on both the waves which are on the order of or smaller than the radar footprint (the Bragg waves) and on the underlying tilt imposed from waves with wavelengths much larger than the radar footprint (gravity waves). For the former case of shorter wavelength waves, σ° is considered constant but the instantaneous amplitude of the return varies, yielding the conditional probability $p(a|\sigma^\circ)$. For the latter case of longer wavelength waves due to incidence angle and hydrodynamic modulation by long wavelength waves, σ° is allowed to vary with probability $p(\sigma^\circ)$. The amplitude distribution may then be expressed as the conditional probability

$$p(a) = \int_0^\infty p(a|\sigma^\circ) p(\sigma^\circ)\, d\sigma^\circ. \tag{2}$$

The probability of measuring a given backscatter amplitude a can be calculated by considering distributions on the orders of both scales.

1) Distribution of $p(a|\sigma^\circ)$: When the scatterometer footprint is large, the scattered fields should be normally distributed via the central limit theorem. In this case, the amplitude a of the radar return should be Rayleigh distributed [7]. On the other hand, when the scatterometer footprint is on the order of the intermediate to large sized waves, this assumption is less valid, but should still hold if the footprint encompasses several

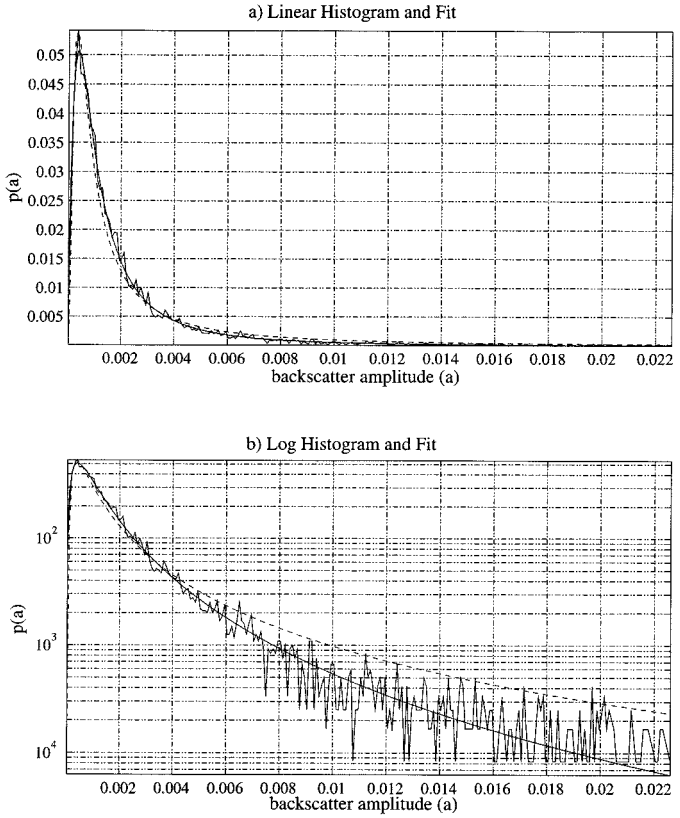

Fig. 1. "Best" fit Rayleigh/generalized lognormal distribution (R/gln) for data at 5 GHz, h-pol, downwind, 30° incidence angle, and wind speed 5 m/s plotted on (a) linear and (b) log scales. Estimated R/gln distribution parameter values are $a_1 = 20.81$, $a_2 = -26.32$, and $C = 4.4712\text{e}5$. The solid smooth line is the best fit R/gln distribution, while the solid jagged line is the data histogram. The dashed line is the best fit Weibull distribution.

correlation lengths [2]. This conclusion has been previously debated [8], [9], with Gotwols and Thompson [2] concluding that for their small footprint data, $p(a|\sigma^\circ)$ is indeed Rayleigh distributed. Due to the similarity of the footprint size, the present analysis assumes that $p(a|\sigma^\circ)$ is Rayleigh distributed for YSCAT94 data based on the previous theoretical justification and the experimental results in [2]. Because Gotwols and Thompson's analysis is for midrange incidence angles, this assumption may be less valid for YSCAT observation angles of 0°, 10°, and 60°.

2) Distribution of $p(\sigma^\circ)$: In order to completely determine σ° in (1), expressions must be found for the reflection coefficients g_{pp} and the wave number spectrum $\Psi(2k_m \sin\theta_i, 0)$. Using the reflection coefficients derived from SPT (see [5]) and a simple $\Psi \approx k^{-4}$ Phillip's spectrum, Gotwols and Thompson noted the linear nature of the h-pol σ° and the quadratic nature of the v-pol σ° return in log space as a function of wave slope for their pathological case of 45° incidence. Accordingly, for the general case, they proposed the following model for σ° versus wave slope s_x

$$\sigma_p^\circ = Ce^{a_1 s_x + a_2 s_x^2} \tag{3}$$

where p is either v or h for v-pol and h-pol respectively. From (3) we can find an expression for $p(\sigma_p^\circ)$ by applying the transformation law for probability density

$$p(\sigma_p^\circ) = \frac{p(s_x)}{|d\sigma_p^\circ/ds_x|}. \tag{4}$$

Assuming that the wave slope distribution $p(s_x)$ is a normal distribution with variance σ_x^2 and zero mean and noting that

$$\begin{aligned} |d\sigma_p^\circ/ds_x| &= C(a_1 + 2a_2 s_x)e^{a_1 s_x + a_2 s_x^2} \\ &= (a_1 + 2a_2 s_x)\sigma_p^\circ \end{aligned} \tag{5}$$

and from (3)

$$s_x = \frac{-a_1 \pm \sqrt{a_1^2 + 4a_2 \ln\left(\dfrac{\sigma_p^\circ}{C}\right)}}{2a_2} \tag{6}$$

it can be shown that for $a_2 = 0$, [2]

$$p(\sigma^\circ) = \frac{1}{a_1 \sigma_x \sigma^\circ \sqrt{2\pi}} \exp\left\{\frac{-(\ln\sigma^\circ - lnC)^2}{2a_1^2\sigma_x^2}\right\} \tag{7}$$

$$\begin{aligned} p(a) &= \int_0^\infty \underbrace{p(a|\sigma^\circ)}_{\text{Rayleigh}} \underbrace{p(\sigma^\circ)}_{(8)}\, d\sigma^\circ \\ &= \int_0^\infty \underbrace{\frac{2a\sigma^\circ}{e^{a^2\sigma^\circ}}}_{p(a|\sigma^\circ)} \underbrace{\left(\frac{\exp\left(\dfrac{a_1^2}{4\sigma_x^2 a_2^2}\right) \exp\left(\pm\dfrac{a_1\sqrt{a_1^2 + 4a_2 \ln\dfrac{\sigma^\circ}{C}}}{4\sigma_x^2 a_2^2}\right) \left(\dfrac{\sigma^\circ}{C}\right)^{\left(\frac{1}{2a_2\sigma_x^2}\right)}}{\sigma_x \sigma^\circ \sqrt{\pi}\sqrt{a_1^2 + 4a_2 \ln\frac{\sigma^\circ}{C}}} \right)}_{p(\sigma^\circ)[(8)]} d\sigma^\circ \end{aligned} \tag{9}$$

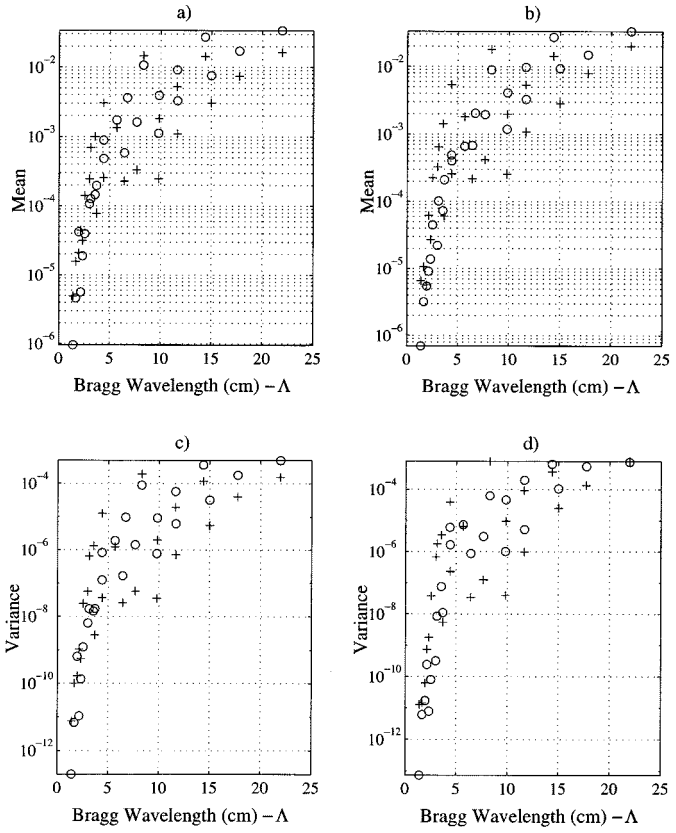

Fig. 2. Aggregate amplitude mean (μ) and variance (σ^2) of YSCAT94 amplitude measurements according to Bragg wavelength (Λ) for a fixed wind speed of 4 m/s [(a) and (b)] and for a fixed wave slope [(c) and (d)]. Circles indicate v-pol, upwind values. Pluses indicate h-pol, upwind values.

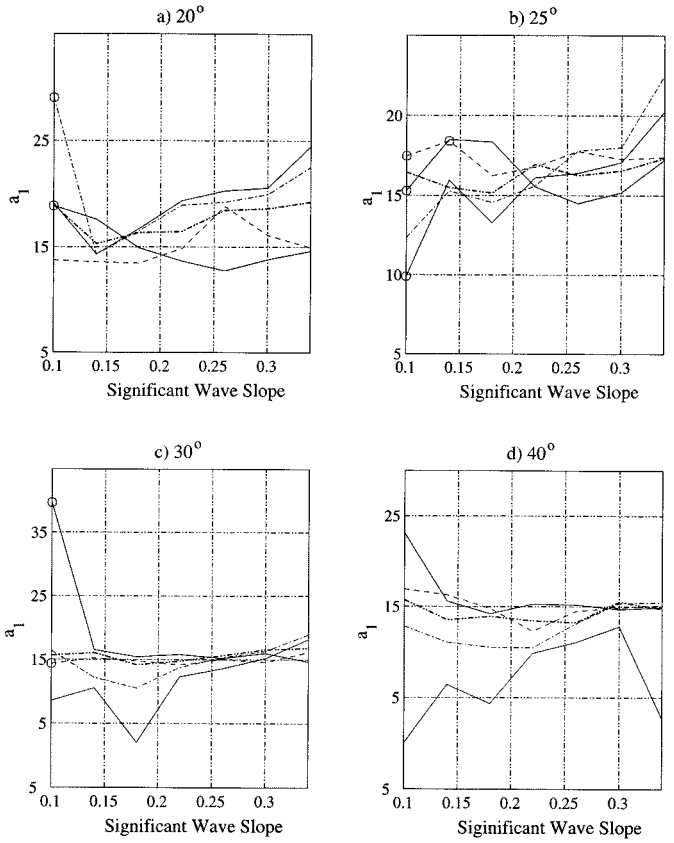

Fig. 3. $|a_1|$ values versus significant wave slope. (a) 20°, (b) 25°, (c) 30°, and (d) 40° incidence angle. Data is for v-pol, downwind case. The thin solid line corresponds to 2 GHz, dashed line corresponds to 3 GHz, dotted line corresponds to 5 GHz, dash/dot line corresponds to 10 GHz, and the bold solid line corresponds to 14 GHz. Circles indicate bins with only one or two minutes of data.

and for the more general case of $a_1,\ a_2 \neq 0$ [10]

$$p(\sigma^\circ(s_x)) = \frac{1}{\sigma_x(a_1 + 2a_2 s_x)Ce^{a_1 s_x + a_2 s_x^2}\sqrt{2\pi}} \cdot \exp\left\{\frac{-(s_x)^2}{2\sigma_x^2}\right\} \quad (8)$$

with s_x as defined by (6) and for $s_x \rightarrow N(0,\ \sigma_x)$. The pdf in (7) is referred to as the lognormal distribution. The pdf described by (8), was first identified in [11] as the generalized lognormal distribution and is the focus of the next section. From (2), $p(\sigma^\circ)$ may be modeled by (7) for $a_2 = 0$ and (8) for $a_1,\ a_2 \neq 0$.

For the more general case of $a_1,\ a_2 \neq 0$, (2) becomes (9), shown at the bottom of the previous page, where polarization dependence has been dropped for notational convenience. Using (3) and (4), (9) may also be written in terms of s_x as

$$p(a) = \int_0^\infty \underbrace{p(a|\sigma^\circ(s_x))}_{\text{Rayleigh}} \underbrace{p(s_x)}_{N(0,\sigma_x)}\, d\sigma^\circ = \int_{-\infty}^\infty \underbrace{2aCe^{a_1 s_x + a_2 s_x^2} e^{-a^2 Ce^{a_1 s_x + a_2 s_x^2}}}_{p(a|\sigma^\circ(s_x))} \underbrace{\frac{e^{-s_x^2/2\sigma_x^2}}{\sqrt{2\pi}\sigma_x}}_{p(s_x)}\, ds_x. \quad (10)$$

Equation (10) provides a model which describes the pdf of the radar backscatter amplitude from the sea surface at midrange incidence angles. More is said about this distribution in Section III-C.

B. Generalized Lognormal Distribution

The generalized lognormal distribution is defined in terms of s_x by (8) or in terms of σ° [using (3)] as in (11), shown at the bottom of the next page. Four parameters, a_1, a_2, C, and σ_x, dictate the distribution function produced by (11). However, the distribution can be degenerate (i.e., it has nonunique solutions) when all four parameters are left free. In order to contrast a_1, a_2, and C values for different data bins, this problem of degeneracy is alleviated by fixing σ_x to be the representative slope standard deviation (σ_x) of 0.0914. This value of the slope standard deviation was chosen from the σ_x population calculated from wire wave gauge data [10] recorded at the CCIW site. The absolute values of a_1, a_2, and C are dependent on this fixed σ_x. However, the relative values of these three parameters is comparable to other studies because the *shape* of the generalized lognormal distribution is dependent only upon the relative a_1 and a_2 [11].

To aid in the comparison of YSCAT94 data with (10), the mean and variance of the generalized lognormal distribution

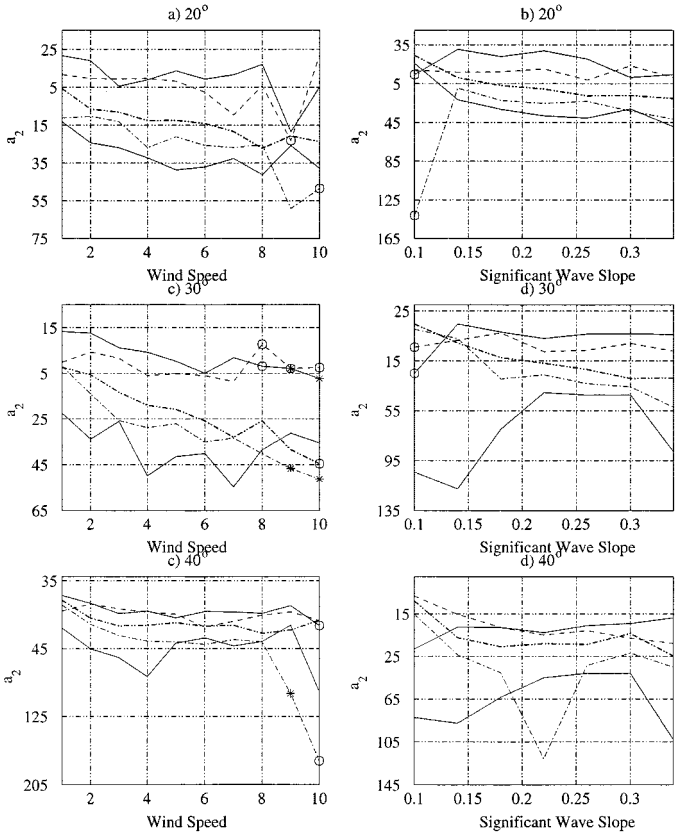

Fig. 4. a_2 values versus wind speed and significant wave slope. (a), (b) 20°, (c), (d) 30°, and (e) and (f) 40° incidence angle. Data is for v-pol, downwind case. The thin solid line corresponds to 2 GHz, the dashed line corresponds to 3 GHz, the dotted line corresponds to 5 GHz, dash/dot line corresponds to 10 GHz, and the bold solid line corresponds to 14 GHz. Asterisks correspond to bins with no data, and circles indicate bins with only one or two minutes of data.

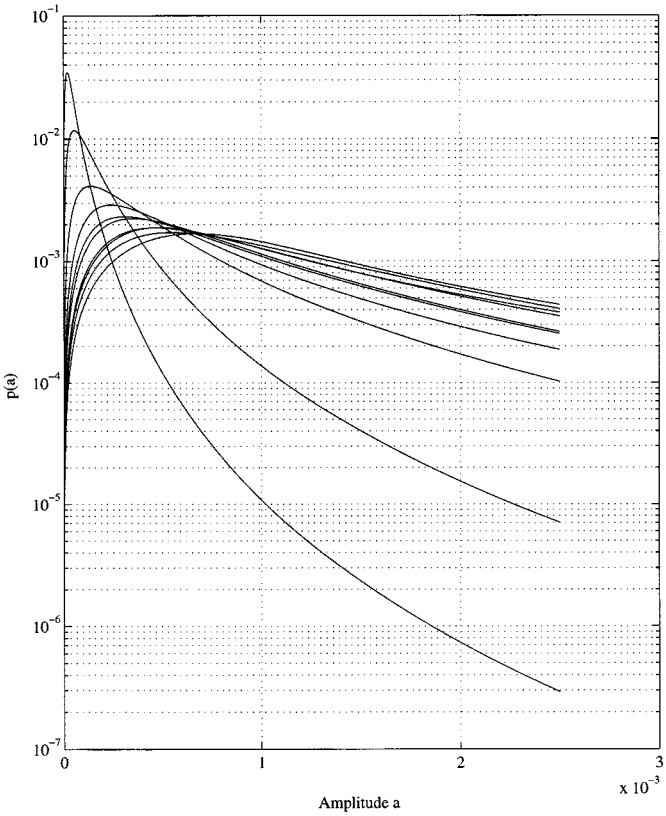

Fig. 5. Distribution shape progression for the Rayleigh/generalized lognormal distribution according to wind speed. Data is for 10 GHz, v-pol, downwind, 20°, and wind speed 1–10 m/s. Distribution with the lowest tail is for 1 m/s wind speed, highest tail is 10 m/s.

(11) are derived as shown at the bottom of the page. The mean is given by (12), shown at the bottom of the next page. Using the change of variables

$$u = \sqrt{a_1^2 + 4a_2 \ln \frac{\sigma^\circ}{C}}$$

with

$$du = \frac{2a_2}{\sigma^\circ \sqrt{a_1^2 + 4a_2 \ln \frac{\sigma^\circ}{C}}}. \tag{13}$$

Equation (12) may be written as (14), shown at the bottom of the next page, and thus the mean of the generalized lognormal distribution is given by

$$\mu_{g\ln} = \frac{C \exp\left(\frac{a_1^2 \sigma_x^2}{1 - 2a_2\sigma_x^2}\right)}{\sqrt{1 - 2a_2\sigma_x^2}}. \tag{15}$$

By a similar method, the variance may be written as

$$\sigma_{g\ln}^2 = \frac{C^2 \exp\left(\frac{2a_1^2 \sigma_x^2}{1 - 4a_2\sigma_x^2}\right)}{\sqrt{1 - 4a_2\sigma_x^2}}. \tag{16}$$

Note that the same distribution is generated regardless of the sign of a_1. Also note that the parameter a_1 appears only as a

$$p(\sigma^\circ) = \frac{\exp\left(\frac{a_1^2}{4\sigma_x^2 a_2^2}\right) \exp\left(\pm \frac{a_1 \sqrt{a_1^2 + 4a_2 \ln \frac{\sigma^\circ}{C}}}{4\sigma_x^2 a_2^2}\right) \left(\frac{\sigma^\circ}{C}\right)^{(1/2a_2\sigma_x^2)}}{\sigma_x \sigma^\circ \sqrt{\pi} \sqrt{a_1^2 + 4a_2 \ln \frac{\sigma^\circ}{C}}} \tag{11}$$

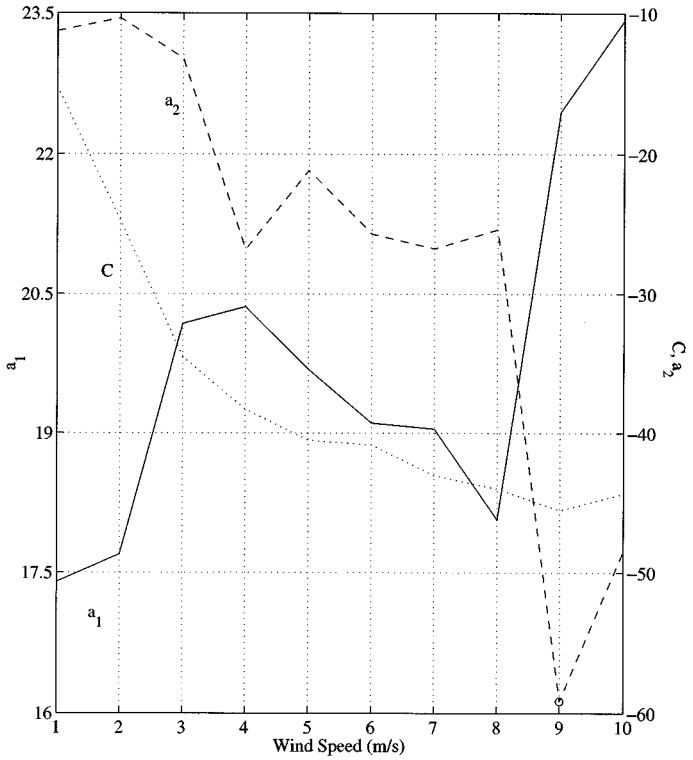

Fig. 6. a_1, a_2, and C values for the Rayleigh/generalized lognormal distribution for 10 GHz, v-pol, downwind, 20°, wind speed 1–10 m/s. C values are scaled by the relation $20\log_{10}(C) - 100$. Solid line represents a_1 values. Dashed line represents a_2 values. Dotted line represents C values.

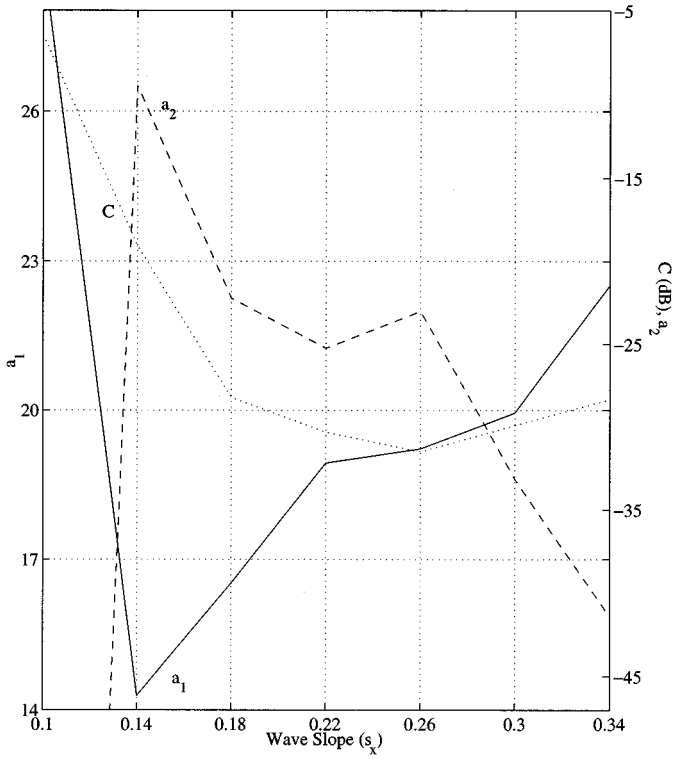

Fig. 7. a_1, a_2, and C values for the Rayleigh/generalized lognormal distribution for 10 GHz, v-pol, downwind, 20°, significant wave slope 0.1–0.34. C values are scaled by the relation $20\log_{10}(C) - 100$. Solid line represents a_1 values. Dashed line represents a_2 values. Dotted line represents C values.

squared quantity in (15) and (16). Due to this, in Section IV the absolute value of a_1 is plotted instead of a_1.

C. Rayleigh/Generalized Lognormal Distribution

The distribution defined by (10) is referred to in this paper as the Rayleigh/generalized lognormal (R/gln) distribution. An analytical solution to this integral is not known by the authors. However, (10) may be successfully integrated numerically over all possible wave slopes s_x for a given set of parameters C, a_1, and a_2 and for a specific value of backscatter amplitude a. Amplitude probability distributions $p(a)$ produced in this manner may be fit to histograms generated from YSCAT94 10 Hz sampled raw data records [10] for each data case using the Kullback–Leibler distance between two probability distributions [12]

$$p(f||g) = \sum_{n=-\infty}^{\infty} \left| f(x_n) \log \frac{f(x_n)}{g(x_n)} \right|. \tag{17}$$

By minimizing (17), C, a_1, and a_2 values are determined for each YSCAT94 case according to frequency, polarization, wind direction, incidence angle, wind speed, and estimated significant wave slope. An example fit of the R/gln is shown in Fig. 1.

$$\mu_{g\ln} = \lim_{a\to\infty} \int_0^a \frac{\exp\left(\frac{a_1^2}{4\sigma_x^2 a_2^2}\right) \exp\left(\pm \frac{a_1\sqrt{a_1^2 + 4a_2 \ln \frac{\sigma^\circ}{C}}}{4\sigma_x^2 a_2^2}\right) \left(\frac{\sigma^\circ}{C}\right)^{(1/2a_2\sigma_x^2)}}{\sigma_x \sigma^\circ \sqrt{\pi}\sqrt{a_1^2 + 4a_2 \ln \frac{\sigma^\circ}{C}}} \sigma^\circ \, d\sigma^\circ. \tag{12}$$

$$\mu_{g\ln} = \lim_{a\to\infty} \int_0^a \frac{C \exp\left(\frac{u^2(2\sigma_x a_2 - 1) + u(2a_1) - (a_1^2 + 2a_2\sigma_x^2 a_1^2)}{8\sigma_x^2 a_2^2}\right)}{\sigma_x a_2 2\sqrt{2\pi}} du. \tag{14}$$

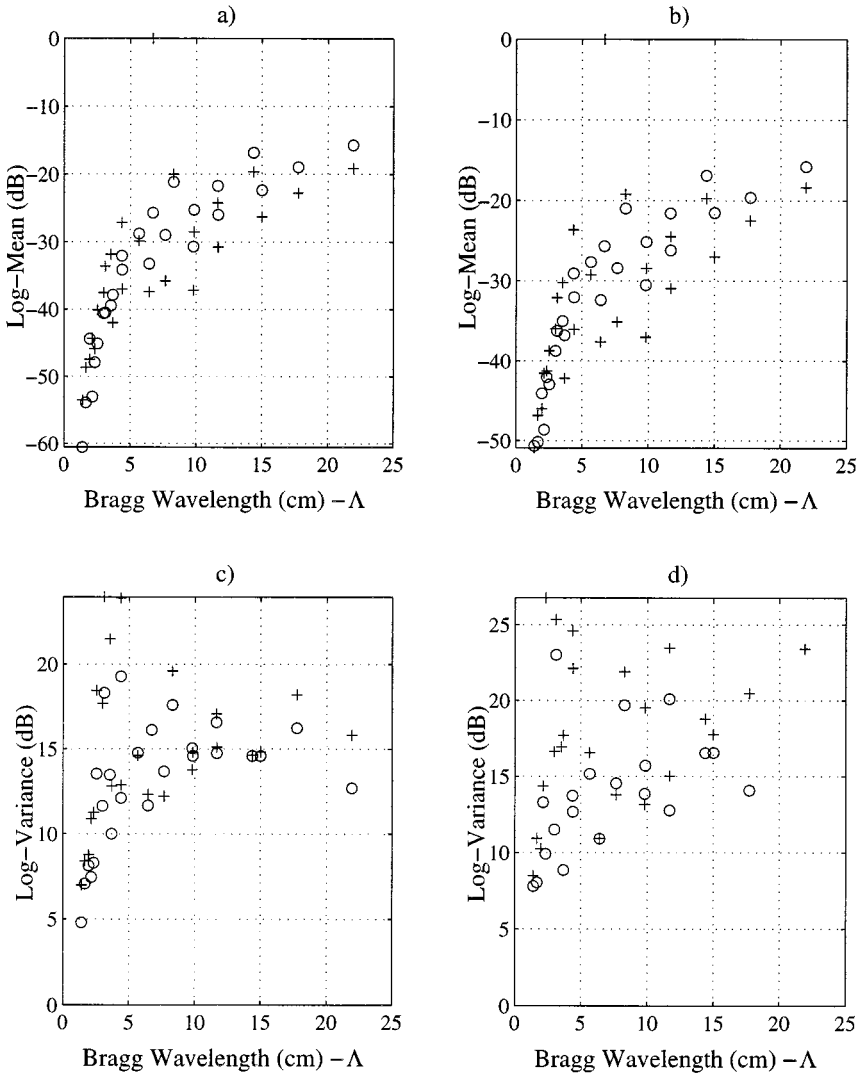

Fig. 8. Log-mean (μ) and log-variance (σ^2) according to Bragg wavelength (Λ). (a) and (b) show the mean according to the Bragg wavelength for (a) wind speed of 4 m/s and (b) significant wave slope of 0.2. (c) and (d) show the log-variance according to the Bragg wavelength for the same cases. Circles indicate v-pol, upwind values. Pluses indicate h-pol, upwind values.

The fit produced by the R/gln is excellent even in the tails while a best fit Weibull distribution does not model the high amplitude portion of $p(a)$ as accurately. C, a_1, and a_2 results calculated in this manner for the more than one thousand data cases are discussed in Section IV.

IV. Results

Fitting the R/gln distribution to the YSCAT94 data results in the distribution parameters which describe the behavior of the instantaneous amplitude backscatter distributions $p(a)$ of the YSCAT94 data set. Some statements about trends visible in the R/gln parameters, and specific examples from a few select cases are presented here. For a more exhaustive report of these results, the reader is referred to [10].

Each R/gln parameter displays general trends when tabulated versus environmental parameters. For example, the mean backscatter amplitude for each data case exhibits a general trend of increasing with wind speed and significant wave slope, though the increase is more gradual with significant wave slope. In general, the higher the frequency and the higher the incidence angle (i.e., the smaller the Bragg wavelength Λ), the lower the mean amplitude. The same (very) general statements may be given for the variance of the amplitude measurements for each data case, although for both the mean and variance a decreasing trend can be observed for 0° (nadir) scattering, especially at higher frequencies. Fig. 2 shows the amplitude mean and variance for different Bragg wavelengths.

In general, C values display trends reversed from those of the amplitude mean and variance. C values tend to decrease according to a log relationship with wind speed and significant wave slope with the exception of 0° (nadir) cases, which display a slight tendency to increase. It should be remembered, however, that the model under consideration has no theoretical justification at very low incidence angles and therefore model parameters in this regime should be viewed accordingly.

R/gln a_1 values tend to stay in the same range of 5–25 for different frequencies and incidence angles. A slight upward trend can be seen in many cases when plotted versus significant wave

slope as in Fig. 3. A similar relationship is observed when these quantities are tabulated according to wind speed [10].

R/gln a_1 values also tend to decrease as incidence angle increases, as can be seen in Fig. 3. R/gln a_2 values display a decreasing trend when considered versus wind speed and significant wave slope. These a_2 values tend to be lower for smaller Bragg wavelengths (higher frequencies and increasing incidence angles) as illustrated in Fig. 4. A typical progression of the backscatter distributions for incidence angles of 0° (nadir)—60° is shown graphically in Figs. 5–7. For the case of 5 GHz, vertical polarization, downwind, and 20° incidence angle, Fig. 5 shows how the distribution shape changes as wind speed changes, Fig. 6 shows the relationship between R/gln a_1, a_2, and C parameters and wind speed, while Fig. 7 shows the relationship of these same parameters according to significant wave slope.

The statistics of the data after taking the log of each amplitude measurement also display an interesting behavior. While the log-mean values rise in a similar fashion to the linear mean, the log-variance exhibits only poorly defined trends for a given frequency, polarization, incidence angle, and wind direction. This can be seen in Fig. 8 by plotting the log-mean and log-variance (mean and variance of the log of the amplitude measurements) versus the Bragg wavelength (Λ). This failure of the log-variance to increase with increasing wind speed has been noticed by others and a possible explanation for this phenomenon is given in [13].

V. Conclusion

Following Gotwols and Thompson [2], the probability distribution function for the amplitude of the backscatter was calculated based on conditional probabilities (2). For YSCAT94 data, $p(a|\sigma^\circ)$ was assumed to be Rayleigh distributed, and the distribution for $p(\sigma^\circ)$ was theoretically shown to be the generalized lognormal distribution for midincidence angles. This model was based on a second degree polynomial in log space which approximated the normalized radar cross section (σ°) predicted by the composite model of a sea containing waves generated by a simple Phillips power spectrum. The resulting Rayleigh/generalized lognormal distribution derived from (2) was fit to YSCAT94 empirical amplitude data distributions. The goodness of the fit demonstrates validity of this model especially for midrange incidence angle backscatter. Trends in the Rayleigh/generalized lognormal distribution parameters a_1, a_2, and C were identified. C displayed a very distinct trend with an inverse relationship to the mean: data cases with greater means corresponded to smaller values for C. The a_1 and a_2 parameters also displayed trends when considered versus wind speed and significant wave slope.

Acknowledgment

The authors wish to thank M. Donelan for permitting them to use wave staff data from his experiments and the Canada Centre for Inland Waters (CCIW), Burlington, ON, Canada, for permitting them to deploy YSCAT at the WAVES research platform in 1994.

References

[1] M. A. Donelan and W. J. Pierson, "Radar scattering and equilibrium ranges in wind generated waves with application to scatterometry," *J. Geophys. Res.*, vol. 92, no. C5, pp. 4971–5029, May 1987.
[2] B. L. Gotwols and D. R. Thompson, "Ocean microwave backscatter distributions," *J. Geophys. Res*, vol. c5, no. 99, pp. 9741–9750, May 1994.
[3] D. G. Long, R. S. Collyer, R. Reed, and D. V. Arnold, "Dependance of the normalized radar cross section of water waves on Bragg wavelength—Wind speed sensitivity," *IEEE Trans. Geosci. Remote Sensing*, vol. 34, pp. 656–666, Mar. 1996.
[4] R. Reed, "Statistical properties of the sea scattered radar return," Ph.D. dissertation, Brigham Young Univ., Provo, UT, Dec. 1995.
[5] W. J. Plant, "Bragg scattering of electromagnetic waves from the air–sea interface," in *Surface Waves and Fluxes*, G. L. Geernaert and W. J. Plant, Eds. Norwell, MA: Kluwer, 1990.
[6] G. R. Valenzuela and M. B. Laing, "On the statistics of sea clutter," Tech. Rep. 7349, U.S. Naval Res. Lab., Washington, DC, 1971.
[7] H. R. Raemer, *Radar Systems Principles*. Boca Raton, FL: CRC, 1997.
[8] G. V. Trunk, "Radar properties of non-Rayleigh sea clutter," *IEEE Trans. Aerosp. Electron. Syst.*, vol. AES-8, pp. 196–204, Mar. 1972.
[9] K. D. Ward, C. J. Baker, and S. Watts, "Maritime surveillance radar, 1, radar scattering from the ocean surface," *Proc. Inst. Elect. Eng. F*, vol. 137, pp. 51–62, Jan. 1990.
[10] B. E. Barrowes, "YSCAT backscatter distributions," M.S. thesis, Brigham Young Univ., Provo, UT, 1999.
[11] B. L. Gotwols, R. D. Chapman, and R. E. Sterner, II, "Ocean radar backscatter statistics and the generalized log normal distribution," in *Proc. PIERS*, J. A. Kong, Ed. Boston, MA, July 1994.
[12] T. M. Cover and J. M. Thomas, *Elements of Information Theory*. New York: Wiley, 1990.
[13] P. H. Dahl and W. J. Plant, "The variability of high-frequency acoustic backscatter from the region near the sea surface," *J. Acoust. Soc. Amer.*, vol. 101, pp. 2595–2602, May 1997.

Benjamin E. Barrowes received the B.S. and M.S. degrees in electrical engineering from Brigham Young University, Provo, UT, both in 1999, and is currently pursuing the Ph.D. degree in electrical engineering from the Massachusetts Institute of Technology, Cambridge.

His research interests include wind–wave interaction and electromagnetic wave scattering from the sea surface and from random media.

David G. Long (M'79–SM'98) received the Ph.D. degree in electrical engineering from the University of Southern California, Los Angeles, in 1989.

From 1983 to 1990, he worked for NASA's Jet Propulsion Laboratory, Pasadena, CA, where he developed advanced radar remote sensing systems. While at JPL, he was Project Engineer on the NASA Scatterometer (NSCAT) Project, which flew from 1996 to 1997. He also managed the SCANSCAT project, the precursor to SeaWinds that was first flown in 1999. He is currently a Professor in the Electrical and Computer Engineering Department, Brigham Young University, Provo, UT, where he teaches upper division and graduate courses in communications, microwave remote sensing, radar, and signal processing. He is the Principle Investigator on several NASA-sponsored research projects in remote sensing. He has numerous publications in signal processing and radar scatterometry. His research interests include microwave remote sensing, radar theory, space-based sensing, estimation theory, signal processing, and mesoscale atmospheric dynamics.